의학석사 학위논문

Diagnostic value of Integrated PET/MRI for Detection and Localization of Prostate Cancer: Comparative Study to Multiparametric MRI and PET/CT

일체형 PET/MRI의 전립선암 병변 검출 및 국소화에 대한 진단적 가치: 다변수 자기공명영상과 PET/CT 와의 진단능 비교 연구

2015 년 1 월

서울대학교 대학원

의학과 영상의학 전공

이 명 석

A Thesis of the Degree of Master of Science in Medicine

일체형 PET/MRI의 전립선암 병변 검출 및 국소화에 대한 진단적 가치: 다변수 자기공명영상과 PET/CT 와의 진단능 비교 연구

Diagnostic value of Integrated PET/MRI for Detection and Localization of Prostate Cancer: Comparative Study to Multiparametric MRI and PET/CT

January 2015

The Department of Radiology

Seoul National University

College of Medicine

Myoung Seok Lee

일체형 PET/MRI의 전립선암 병변 검출 및 국소화에 대한 진단적 가치: 다변수 자기공명영상과 PET/CT 와의 진단능 비교 연구

지도교수 조 정 연

이 논문을 이 명 석 의 석사학위논문으로 제출함

2015년 1월

서울대학교 대학원

의학과 영상의학 전공

이 명 석

이 명 석 의 석사학위논문을 인준함

2015년 1월

위 원 장 김 승 협 (인)

부 위 원 장 조 정 연 (인)

위 원 천 기 정 (인)

Diagnostic value of Integrated PET/MRI for Detection and Localization of Prostate Cancer: Comparative Study to Multiparametric MRI and PET/CT

By

Myoung Seok Lee, M.D.

Director: Prof. Jeong Yeon Cho, M.D., Ph.D.

A thesis submitted to the College of of Medicine in partial fulfillment of the requirements for the degree of Master of Science in medicine (Radiology)

in Seoul National University , Seoul, Korea

January 2015

Approved by Thesis Committee:

Professor Seung Hyup Kim, Chairman

Professor Jeong Yeon Cho, Vice chairman

Professor Gi Jeong Cheon

Abstract

Purpose: To evaluate the diagnostic value of integrated PET/MRI compared with conventional multiparametric MRI and PET/CT for the detailed and accurate segmental detection/localization of prostate cancer.

Methods: Thirty-one patients who underwent integrated PET/MRI using ^{18}F-choline and ^{18}F-FDG with an integrated PET/MRI scanner followed by radical prostatectomy were included. The prostate was divided into 6 segments (sextants) according to anatomical landmarks. Three board-certified radiologists noted the presence and location of cancer in each sextant on four different image interpretation modalities in consensus (1, multiparametric MRI; 2, integrated ^{18}F-FDG PET/MRI; 3, integrated ^{18}F-choline PET/MRI; and 4, combined interpretation of 1 and ^{18}F-FDG PET/CT). Sensitivity, specificity, accuracy, positive and negative predictive values, likelihood ratios, and diagnostic performance based on the DOR (diagnostic odds ratio) and NND (number needed to diagnose) were evaluated for each interpretation modality, using the pathologic result as the gold standard. Detection rates of seminal vesicle invasion and extracapsular invasion were also evaluated.

Results: Integrated ^{18}F-choline PET/MRI showed significantly higher sensitivity

than did multiparametric MRI in all patients and low Gleason score patients. Integrated ^{18}F-choline PET/MRI and ^{18}F-FDG PET/MRI showed similar sensitivity and specificity to combined interpretation of multiparametric MRI and ^{18}F-FDG PET/CT. However, integrated ^{18}F-choline PET/MRI showed the best diagnostic performance among the imaging modalities, regardless of Gleason score. Integrated ^{18}F-choline PET/MRI showed higher sensitivity and diagnostic performance than did integrated ^{18}F-FDG PET/MRI.

Conclusion: Integrated PET/MRI carried out using a dedicated integrated PET/MRI scanner provides superior accuracy and diagnostic value for detection/localization of prostate cancer. Generally, integrated ^{18}F-choline PET/MRI shows better accuracy and diagnostic performance than does integrated ^{18}F-FDG PET/MRI.

Keywords: Magnetic resonance imaging, Positron emission tomography, Integrated PET/MRI, Prostate cancer, Multiparametric imaging, Diagnostic value

Student Number: 2010-21812

Contents

List of Tables and Figures

List of Abbreviations

FDG = Fluorodeoxyglucose

MRI = Magnetic Resonance Imaging

PET = Positron Emission Tomography

TRUS = Transrectal Ultrasound

DWI = Diffusion-Weighted Imaging

ADC = Apparent Diffusion Coefficient

DCE = Dynamic Contrast-Enhanced imaging

AC = Attenuation Correction

PLND = Pelvic Lymph Node Dissection

DOR = Diagnostic Odds Ratio

NND = Number Needed to Diagnose

Introduction

Prostate cancer was the 4th most common cancer worldwide in 2012, accounting for 7.9% of the total number of new cases (1,112,000 new cases) and the 2nd most common cancer diagnosis in men (*1*). In Korea Republic, 8952 men were newly diagnosed with prostate cancer in 2011, representing the 7th most common cancer for all Koreans (7.6%) and the 5th for Korean men (8.1%) (*2*).

Small prostate cancers with organ confinement (T1 or T2a) usually have low Gleason scores and low prostate-specific antigen (PSA) levels (≤10), and probably can be managed with active surveillance (*3*). Recently, minimally invasive therapies such as radiofrequency ablation (RFA), brachytherapy, and high-intensity focused ultrasonography (HIFU) have helped provide uncompromised oncologic outcome with significantly less comorbidity (*4*). Therefore, accurate characterization of tumor location and extent is important in the application of suitable emerging focal therapies, and may also impact patient management during active surveillance (*5*).

Detection and localization of prostate cancer foci are thus becoming increasingly important, and magnetic resonance imaging (MRI) is generally considered the best modality for this purpose. Soft-tissue contrast can be depicted with MRI, and an important role of this modality is to distinguish organ-confined tumors from capsule-penetrating tumors. Beside conventional T2-weighted imaging (T2WI), techniques that can reveal physiological properties such as diffusion-weighted

imaging (DWI), dynamic contrast-enhanced imaging with subtraction (DCE), and MR spectroscopy (MRS) may reinforce or complement each other if used in combination (*3*, *5*, *6*).

Positron emission tomography (PET) using conventional ^{18}F-FDG (fluorodeoxyglucose) is known to be of limited use in the detection and localization of prostate cancer because of its low spatial resolution, low sensitivity, and overlapping uptake with benign prostatic hyperplasia (BPH), as well as the relatively low glucose consumption of prostate cancer compared with other cancers (*7*). ^{18}F-FDG PET/CT can add to the anatomic information obtained with PET or MRI, resulting in improved diagnostic performance. However, because prostate cancer is characterized by multiple foci that are often small, PET/CT cannot be used for localization of prostate cancer because of the limited spatial resolution (≥5 mm) and partial volume effect (*8*).

In recent years, radiolabeled choline such as ^{11}C-choline or ^{18}F-choline has been introduced for identification of prostate tumors. PET/CT using ^{11}C-choline showed relatively good diagnostic performance (*9*, *10*). It also showed similar sensitivity, specificity, and accuracy of localization to MRI alone, MRS (*11*), and 12-core transrectal ultrasound (TRUS) guided biopsy (*12*). ^{11}C-choline is good for prostate imaging because of minimal urinary excretion, but it has a short half-life (20 min), making handling difficult, and overlapping uptake with BPH. ^{18}F-choline has similar problems to ^{18}F-FDG, such as accumulation in the bladder and overlapping uptake (*7*). Therefore, despite all the strong points, PET or PET/CT cannot be

considered a first-line tool for diagnosis of prostate cancer in men at risk.

PET/MRI is a new multimodal imaging technique that is expected to improve the diagnostic performance of imaging, especially in cases where soft-tissue evaluation is crucial, such as prostate cancer (*13*). Several studies have been conducted on the application of PET/MRI in the detection and localization of prostate cancer (*14-17*), and some studies have investigated the feasibility of integrated PET/MRI in prostate cancer. However, to our knowledge, there has been no study focused on inter-modality comparison of diagnostic values between integrated PET/MRI (both ^{18}F-FDG and ^{18}F-choline) and other widely used imaging modalities including combined interpretation in an actual clinical setting.

The purposes of our study were to assess the capacity of integrated PET/MRI in the detection and staging of prostate cancer and to evaluate the diagnostic performance of integrated prostate PET/MRI, compared with other imaging interpretation modalities in an actual clinical setting.

Materials and Methods

Study Population

Thirty-five patients who were newly diagnosed with prostate cancer from January 2013 to March 2014 were initially enrolled in the study. All patients were initially detected with high PSA, and the inclusion criteria were patients whose prostate cancer was confirmed by histologic examination of standard TRUS-guided 12-core biopsy samples and who were scheduled to undergo surgery (radical prostatectomy). Exclusion criteria were as follows: (1) negative biopsy result, (2) inoperable prostate cancer due to distant or nodal metastasis or poor general patient condition, (3) renal function too impaired (GFR < 30 mL/min/1.73m^2) to perform contrast-enhanced MRI, and (4) other contraindications for contrast-enhanced MRI. By the exclusion criteria, three patients who did not undergo surgery (two because of the patients' denial and one because of multiple bony metastasis) and one patient who had too small a tumor volume of under 1% on the post-prostatectomy specimen were excluded from the initially enrolled patients. Two patients had a single suspicious lymph node—in the right obturator (Patient 2) and right internal iliac (Patient 13) areas. However, they were included in our study because urologic surgeons decided to perform radical prostatectomy including pelvic lymph node dissection (PLND). Finally, a total of 31 patients were evaluated (mean age, 68.3 years; 95% CI, 64.6–72.8) under approval of our Institutional Review Board and

Ethics Committee. Informed consent was carefully obtained from all patients. We divided them into 2 groups according to pathologic (surgical specimen–based) Gleason score: the high Gleason score group (≥4 + 3; n = 17) and the low Gleason score group (≤3 + 4; n = 14) (*18-20*).

Imaging Procedure and Protocol

All patients underwent ^{18}F-FDG PET/CT and ^{18}F-FDG PET/MRI with a dedicated integrated PET/MR scanner on the same day, at least 2 weeks after TRUS-guided biopsy to avoid pseudolesions from hemorrhage. ^{18}F-fluorocholine PET/MRI was also performed in all patients, with an interval of at least 7 days from ^{18}F-FDG PET/MRI.

On the first examination day, ^{18}F-fluorocholine PET/MRI was performed. The scan was started 15 min after the intravenous injection of ^{18}F-fluorocholine (550 MBq). PET/MRI imaging was performed using an integrated PET/MRI scanner (Biograph mMR; Siemens Healthcare, Erlangen, Germany) designed to acquire PET and MRI data simultaneously. It consists of a 3 T MRI scanner and an inline PET component equipped with a combination of LSO (lutetium oxyorthosilicate scintillation) crystals and APD (avalanche photodiode) detectors. Emission imaging was performed in 3D with an acquisition time of 4 min per bed position (172 × 172 matrix), covering the area from the pelvis to the foramen magnum level. MR imaging was performed simultaneously with the emission imaging. For post-contrast imaging, 0.2 mL/kg meglumine gadotetrate (Dotarem; Guerbet Pharma,

Aulney-Sous-Bois, France) was injected followed by 20 mL saline flush via power injector. The imaging sequence and parameters of the MR are summarized in Table 1. Total imaging time of ^{18}F-fluorocholine PET/MRI was approximately 40 minutes.

On the second examination day, ^{18}F-FDG PET/MRI and ^{18}F-FDG PET/CT were performed. For ^{18}F-FDG PET/MRI, patients fasted for at least 6 hours. Blood glucose levels were checked before FDG administration and were confirmed to be <140 mg/dL. The scan was started 60 min after the intravenous injection of ^{18}F-FDG (5.18 MBq/kg). Some dedicated MR sequences for the prostate were omitted to avoid repeat imaging and to decrease total examination time (Table 1). Total imaging time of ^{18}F-FDG PET/MRI was approximately 30 minutes. PET/CT imaging was performed on a 64-channel multidetector CT scanner (Biograph mCT; Siemens Healthcare, Erlangen, Germany) immediately after ^{18}F-FDG PET/MRI, approximately 90 minutes after ^{18}F-FDG injection. Only pre-contrast images were obtained, with a reconstructed section thickness of 3 mm and 1 mm interval, and a fixed tube voltage of 120 kVp and amperage adjusted by automated tube current modulation.

All the PET/MRI and PET/CT images were analyzed using a workstation equipped with dedicated analysis software (syngo.via; Siemens Medical Solutions, Erlangen, Germany).

Table 1. MR imaging sequences and parameters

Sequence	TR / TE (mSec)	Voxel Size (mm)	Matrix (mm)	FoV (mm)	ST / gap(mm)	FA (degree)
2-point DIXON 3D T1 VIBE Coronal for attenuatuion correction	3.60 / 2.46(in) ~ 1.23(out)	4.1×2.6×3.1	192 × 121		3.12	10
3D T1 FS VIBE axial	3.40 / 1.22	1.6×1.2×3.0	320 x 195	380 x 308	3.0	9
T2 HASTE Whole body Coronal	1200 / 72	1.7×1.2×6.0	384 x 182	450 x 1092	7.8	90
True FISP Localizer						
**** T2 TSE Sagittal Pelvis**	3080 / 116	0.7×0.4×4.0	512 x 317	220 x 220	4.0 / 0.4	130
**** T2 TSE Oblique Coronal**	3000 / 111	0.7×0.5×3.0	448 x 314	220 x 220	3.0 / 0.3	130
**** T2 TSE Oblique Axial**	3080 / 107	0.6×0.4×3.0	448 x 314	199 x 199	3.0 / 0.3	146
**** T1 TSE Oblique Axial**	685 / 9.4	0.9×0.6×3.0	320 x 224	200 x 200	3.0 / 0.3	130
T2 TSE True Axial	3250 / 107	0.6×0.4×3.0	448 x 314	199 x 199	3.0 / 0.3	146
**** Diffusion Weighted Echo Planar 2D Axial**	12600 / 74	1.9×1.9×3.5	160 x 160	300 x 300	3.5 / 0	90

(b=0, 1000)						
**** ADC Map**						
**** Dynamic contrast T1 FS VIBE axial (25 phases)**	4.40 / 1.55	1.1×0.9×3.5 mm	256 x 192	220 x 220	3.5	10
Subtraction images	1st phase was digitally subtracted from the other phases based on dynamic contrast image.					

Abbreviations : VIBE, Volume Interpolated Breath Hold Examination; FS, Fat Suppression; HASTE, Half-Fourier acquisition single-shot turbo spin-echo; True FISP, True fast imaging with steady state free precession; TSE, Turbo Spin Echo; TR, Relaxation Time; TE, Echo Time; FA , Flip angle; FoV, Field of View; ST, Slice thickness. ** : only in 18F-Fluorocholine PET/MRI imaging

Image Analysis

All the MR, PET/MRI, and PET/CT images were carefully and intensely interpreted by three board-certified radiologists in our institution (LMS with 7 years' experience in radiology and 1 years' experience in urogenital radiology, KSY with 11 years' experience in radiology and 4 years' experience in urogenital radiology, and CJY with 21 years' experience in radiology and 17 years' experience in urogenital radiology). The radiologists were completely blinded to biopsy and postoperative pathology results during the image interpretation sessions. The image interpretation consisted of four separate interpretations for different imaging modalities and combinations as followings:

1) Multiparametric MRI: MRI with T2/T1 axial, DCE, and DWI/ADC

2) Integrated ^{18}F-FDG PET/MRI: combined interpretation of MR with DCE and DWI/ADC, gamma camera images, and fused images of PET/MRI

3) Integrated ^{18}F-choline PET/MRI: combined interpretation of MR with DCE and DWI/ADC, gamma camera images of ^{18}F-choline PET, and fused images of PET/MRI

4) Combined interpretation of multiparametric MRI and ^{18}F-FDG PET/CT.

To avoid recall bias, all the four imaging interpretations were performed with a time interval of 7–10 days between each reading session.

The prostate was divided into 6 segments (sextants) according to anatomical landmarks (left/right base, mid, and apex), yielding a total of 186 segments from the 31 patients. During each interpretation, the authors recorded suspected location of cancer based on sextant in consensus. If a lesion lay over multiple sextants, all the involved sextants were considered as suspected cancer-location segments. Seminal vesicle invasion was also evaluated, and involved vesicles were recorded as left or right. Sextants showing extracapsular invasion were specifically aggregated for calculating detection rate, which will be explained later.

In PET/MRI interpretation, MRI-suspect lesions with PET uptake were considered malignant. MRI-positive lesions in the transitional zone without PET uptake were basically considered benign, such as focal inflammatory sequelae, but some cases were considered malignant if the lesions had a definite hyposignal on the ADC map and early enhancement. Lesions in the transitional zone that were PET-positive and MRI-negative were considered benign, such as hyperplasia and adenoma.

The image findings were compared with histopathologic findings of postoperative pathologic specimens. After radical prostatectomy, the prostate was coated with India ink and fixed in 4% buffered formalin. Histologic examination of step-sectioned slices of prostate was performed. After the distal 5 mm portion of the apex was amputated and coned, the prostate was sliced from the base to the apex along the longitudinal axis at 4 mm intervals, followed by paraffin embedding.

Subsequently, microslices were placed on glass slides and stained with hematoxylin-eosin. Seminal vesicles were amputated and submitted separately. A board-certified pathologist (MKC with 17 years' experience) recorded the presence and location of lesions for each of the sextants, as performed by the image interpreters (Figure 1).

(A)

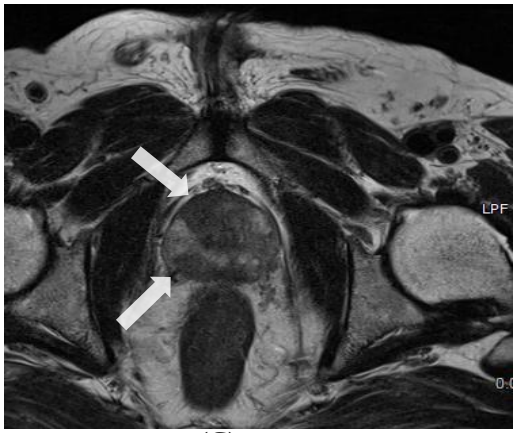

(B)

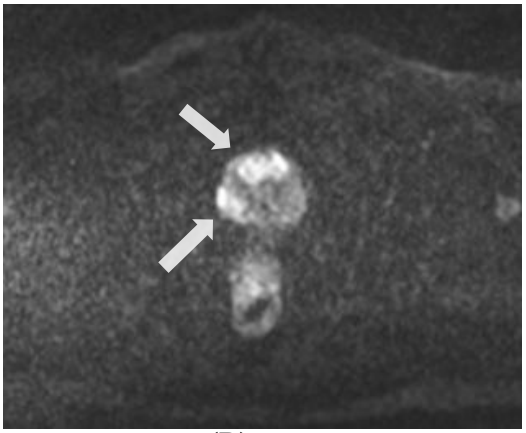

(C)

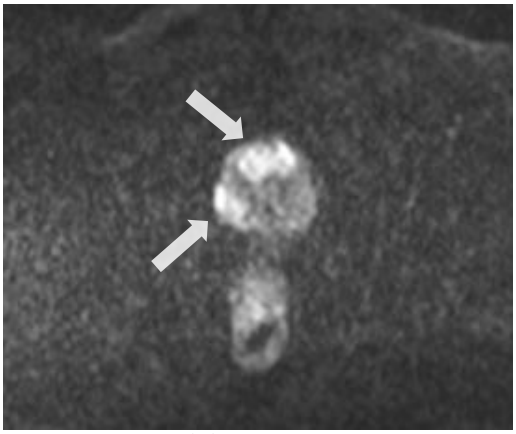

(D)

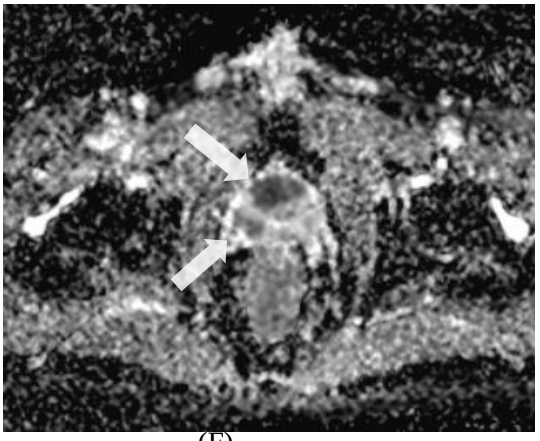

(E)

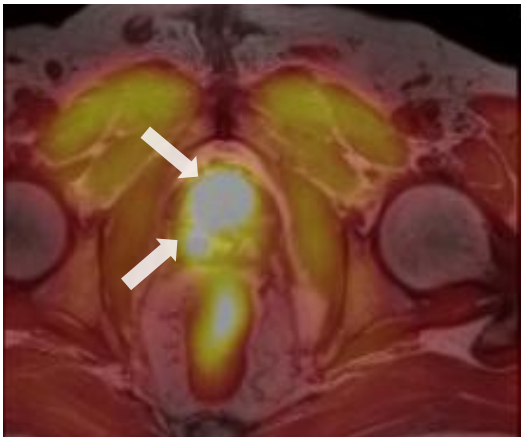

(F)

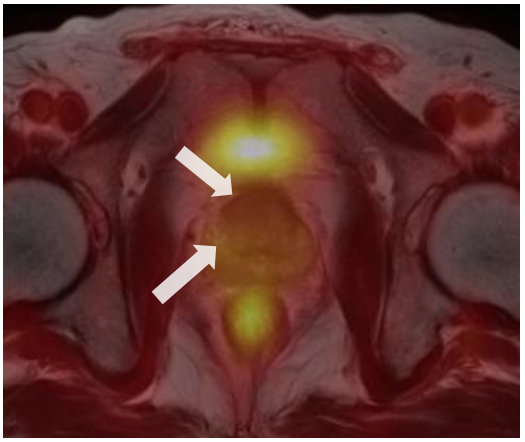

(G) (H)

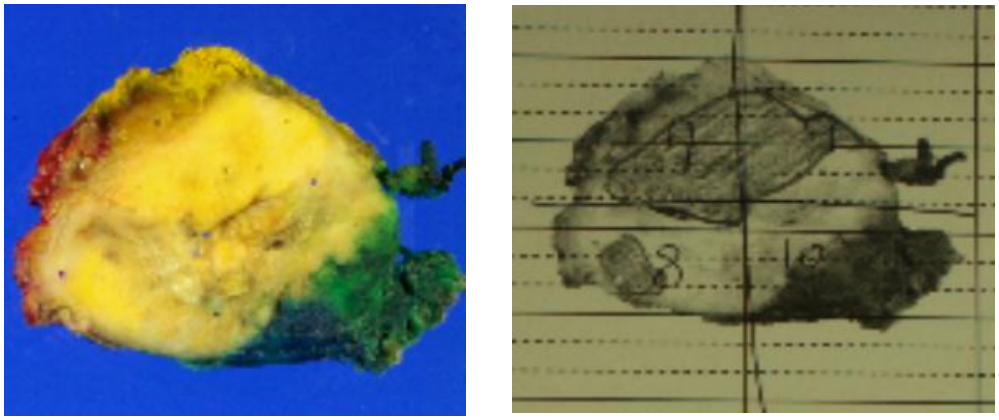

Figure 1. Representative images of relatively high choline uptake on low Gleason score (7, 3+4) prostate cancer lesion

(A) Axial T2-weighted image. There were two focal well-defined low signal intensity lesions at ventral aspect transitional zone and right posterior peripheral zone of mid-gland level of prostate gland. The lesions also showed diffusion restriction on b=1000 image (B), early enhancement on dynamic enhancement series (C), and low ADC value (D). Integrated ^{18}F-choline PET/MRI with image fusion on T2-weighted image (E) showed more prominent radiotracer uptake compared to the fused image of integrated ^{18}F-FDG PET/MRI (F). Surgical specimen (G) and pathologic diagram (F) well presented the lesion and the anatomic allocation of the lesions were very similar to the images.

Statistical analysis

Sensitivity, specificity, positive predictive value (PPV), negative predictive value (NPV), accuracy, positive and negative likelihood ratio (+LR and -LR, respectively) of each interpretation were assessed on sextant-based, regarding the 186 sextants as denominator. Pair-wise comparisons of sensitivity and specificity for each imaging interpretation modalities were performed by using the methodology established by Hawass (21) with Bonferroni method for multiple testing as multiplied by six.

To determine test performance, we used accuracy, diagnostic odds ratio (DOR), and number needed to diagnose (NND) for comparison of diagnostic performance among the imaging interpretation modalities. The DOR was derived from positive and negative likelihood ratios, according to the following equation:

$$\text{DOR} = \frac{TP/FP}{FN/TN} = \frac{(+)LR}{(-)LR} \quad (22)$$

(TP; True positive, FP; False positive, FN; False negative, TN; True positive, (+)LR; Positive likelihood ratio, (-)LR; Negative likelihood ratio)

The NND was calculated from the following equation:

$$\text{NND} = 1/\text{sensitivity} - (1 - \text{specificity}) \quad (23)$$

For evaluation of seminal vesicle invasion, we assessed the accuracy of each imaging interpretation modality, followed by inter-modality comparison using Fisher's exact test. The numbers of sextants showing extracapsular invasion was

small (32 among 186 sections). Thus, we decided to assess the detection rate rather than accuracy for extracapsular invasion. Inter-modality comparison of detection rate for extracapsular invasion was performed using Fisher's exact test.

P values less than or equal to .05 were considered to indicate a significant difference. All statistical analyses were performed with MedCalc software (v. 13.0.4; Ostend, Belgium).

Results

Patient Demographics

The mean age of the patients was 68.3 years, ranging from 51 to 82 years. Mean PSA level was 20.14 (95% CI, 13.03–27.25) ng/mL, ranging from 3.33 to 66.95 ng/mL. All included patients underwent radical prostatectomy successfully without significant immediate complications. Mean tumor volume in prostatectomy specimens was 25.7%, ranging from 4% to 90%. The detailed data are summarized in Table 2.

Table 2. Patients summery

Patient No.	Age(yr)	Initial PSA (ng/dL)	Prostate Volume (mL)	Transitional Zone Volume (mL)	Operation Method	Patholotic Gleason Score
1	76	13.61	28.85	11.82	Retropubic radical prostatectomy	9 (4+5)
2	51	58.18	42.9	20.2	Robot-assisted laparoscopic radical prostatectomy with PLND	7 (4+3)
3	Too small tumor volume under 1%					
4	58	3.33	Outside Biopsy	Outside Biopsy	Robot-assisted laparoscopic radical prostatectomy	7 (4+3)
5	66	25	Outside Biopsy	Outside Biopsy	Robot-assisted laparoscopic radical prostatectomy	7 (3+4)

6	82	36.38	Outside Biopsy	Outside Biopsy	Retropubic radical prostatectomy	8 (4+4)
7	73	28.66	Outside Biopsy	Outside Biopsy	Retropubic radical prostatectomy	7 (4+3)
8	70	7.36	30	16.8	Robot-assisted laparoscopic radical prostatectomy	7 (3+4)
9	68	11	41	16	Robot-assisted laparoscopic radical prostatectomy	7 (3+4)
10	67	3.6	34.62	14.27	Retropubic radical prostatectomy	7 (4+3)
11	73	4.25	73.4	50.8	Robot-assisted laparoscopic radical prostatectomy	6 (3+3)
12	72	4.02	56.3	33.4	Robot-assisted laparoscopic radical prostatectomy	7 (4+3)
13	67	37.21	44.8	28.4	Retropubic radical prostatectomy with PLND	7 (4+3)

14	61	13.25	26	4	Robot-assisted laparoscopic radical prostatectomy	7 (3+4)
15	58	3.91	33.45	12.55	Retropubic radical prostatectomy	6 (3+3)
16	74	45.01	58.2	31.6	Retropubic radical prostatectomy	7 (4+3)
17	70	9.5	37.68	11.12	Robot-assisted laparoscopic radical prostatectomy	9 (4+5)
18	60	21.19	Outside Biopsy	Outside Biopsy	Retropubic radical prostatectomy	7 (3+4)
19	78	4.21	71	50	Retropubic radical prostatectomy	7 (4+3)
20	72	18.4	Outside Biopsy	Outside Biopsy	Robot-assisted laparoscopic radical prostatectomy	7 (4+3)
21	64	24.72	66	34	Retropubic radical prostatectomy	6 (3+3)
22	78	66.95	Outside Biopsy	Outside Biopsy	Retropubic radical prostatectomy	7 (4+3)

23	Operation was denied by patient					
24	72	13.02	38.99	18.34	Robot-assisted laparoscopic radical prostatectomy	7 (3+4)
25	Operation was denied by patient					
26	71	24.94	47.85	25.84	Robot-assisted laparoscopic radical prostatectomy	7 (4+3)
27	Did not undergo operation due to multiple bone metastasis (rib and thoracic vertebrae), converted to hormonal therapy					
28	59	5.6	Outside Biopsy	Outside Biopsy	Robot-assisted laparoscopic radical prostatectomy	7 (4+3)
29	67	8.9	44	25	Robot-assisted laparoscopic radical prostatectomy	7 (4+3)
30	62	4.74	57.5	25.7	Robot-assisted laparoscopic radical prostatectomy	7 (3+4)

31	74	7.9	33.2	20.8	Retropubic radical prostatectomy	7 (3+4)
32	78	8.3	Outside Biopsy	Outside Biopsy	Retropubic radical prostatectomy	9 (5+4)
33	75	8.95	23.32	9.82	Retropubic radical prostatectomy	7 (3+4)
34	65	9.24	53.15	24.32	Robot-assisted laparoscopic radical prostatectomy	7 (3+4)
35	76	4.08	64.3	33.2	Robot-assisted laparoscopic radical prostatectomy	6 (3+3)

Sextant-Based Analysis

The sensitivity, specificity, positive predictive value (PPV), negative predictive value (NPV), accuracy, and positive and negative likelihood ratios (+LR and -LR, respectively) of each interpretation by sextant are described in Table 3.

Generally, integrated ^{18}F-choline PET/MRI provided the best accuracy and sensitivity among the imaging modalities, particularly compared with multiparametric MRI alone. In the total patient group and the low Gleason score group, integrated ^{18}F-choline PET/MRI showed significantly higher sensitivity than did multiparametric MRI alone, even after Bonferroni correction ($p = 0.008 \times 6$ and 0.007×6, respectively) (Table 4).

Combining PET/CT or PET/MRI with multiparametric MRI significantly increased the sensitivity compared with MRI alone, regardless of Gleason score, in each pairwise comparison ($p < 0.05$). However, after the Bonferroni correction in the multimodality comparison, the p values became insignificant (Table 4). There was a tendency for increased accuracy compared with MRI alone, but the difference was small.

Generally, improvements in sensitivity and accuracy were greater with ^{18}F-choline PET/MRI than ^{18}F-FDG PET/MRI. (Table 3-1). Of note, in the total patient group, integrated ^{18}F-choline PET/MRI showed significantly higher sensitivity than ^{18}F-FDG PET/MRI, even after Bonferroni correction (p =

0.003×10^6). These tendencies were well shown in the subgroups—the high and low Gleason score groups (Table 3-2 and 3-3)—and showed statistical significance in each pairwise comparison ($p = 0.016$ and 0.011, respectively). All imaging modalities showed lower sensitivity, specificity, and accuracy in the low Gleason score group than the high Gleason score group.

Table 3. Sensitivity, specificity, PPV, NPV, accuracy and positive and negative likelihood of the study population, grouped as pathologic Gleason score.

3-1. All patients group

([95%CI])	**Multiparametric MRI**	**Integrated ^{18}F-FDG PET/MRI**	**Integrated ^{18}F-choline PET/MRI**	**Multiparametric MRI with ^{18}F-FDG PET/CT**
Sensitivity (%)	58.0 [49.1 , 66.6]	63.4 [54.5 , 64.7]	72.5 [64.0 , 79.9]	68.7 [60.0 , 76.5]
Specificity (%)	87.3 [75.5 , 94.7]	80.0 [67.0 , 89.6]	81.8 [69.1 , 90.9]	72.7 [59.0 , 83.9]
Accuracy (%)	66.7 [60.3 , 70.7]	68.3 [61.6 , 73.4]	75.3 [68.7 , 80.1]	69.9 [63.0 , 75.6]
PPV (%)	91.5 [83.4 , 96.5	88.3 [80.0 , 94.0]	90.5 [83.2 , 95.3]	85.7 [77.5 , 91.8]
NPV(%)	46.6 [36.7 , 56.7]	47.8 [37.8 , 54.5]	55.6 [44.1 , 66.6]	49.4 [38.1 , 60.7]
Positive Likelihood Ratio	4.56 [2.25 , 9.25]	3.17 [1.84 , 5.46]	3.99 [2.25 , 7.06]	2.52 [1.61 , 3.94]
Negative Likelihood Ratio	0.48 [0.38 , 0.60]	0.46 [0.35 , 0.59]	0.34 [0.25 , 0.46]	0.43 [0.32 , 0.58]

3-2. High Gleason score group

([95%CI])	Multiparametric MRI	Integrated ^{18}F-FDG PET/MRI	Integrated ^{18}F-choline PET/MRI	Multiparametric MRI with ^{18}F-FDG PET/CT
Sensitivity (%)	66.2 [54.2 , 76.8]	71.6 [60.0 , 81.5]	77.0 [65.8 , 86.0]	71.6 [60.0 , 81.5]
Specificity (%)	96.4 [81.7 , 99.9]]	85.7 [67.3 , 96.0]	89.3 [71.7 , 97.7]]	78.6 [59.1 , 91.7]
Accuracy (%)	74.5 [66.5 , 76.4]	75.5 [66.5 , 80.7]	80.4 [71.7 , 84.7]	73.5 [64.2 , 80.0]
PPV (%)	98.0 [89.4 , 99.9]	93.0 [83.0 , 98.1]	95.0 [86.1 , 99.0]]	89.8 [79.2 , 96.2]
NPV (%)	51.9 [37.6 , 66.0]	53.3 [37.9 , 68.3]	59.5 [43.3 , 74.4]	51.2 [35.5 , 66.7]
Positive Likelihood Ratio	18.54 [2.69 , 127.93]	5.01 [2.00 , 12.56]	7.19 [2.45 , 21.1]	3.34 [1.62 , 6.89]
Negative Likelihood Ratio	0.35 [0.25 , 0.49]	0.33 [0.22 , 0.49]	0.26 [0.17 , 0.40]	0.36 [0.24 , 0.54]

3-3. Low Gleason score group

([95%CI])	Multiparametric MRI	Integrated ^{18}F-FDG PET/MRI	Integrated ^{18}F-choline PET/MRI	Multiparametric MRI with ^{18}F-FDG PET/CT
Sensitivity (%)	47.4 [34.0 , 31.0]	52.6 [39.0 , 66.0]]	66.7 [52.9 , 78.6]	64.9 [51.1 , 77.1]
Specificity (%)	77.8 [57.7 , 91.4]	74.1 [53.7 , 88.9]	74.1 [53.7 , 88.9]	66.7 [46.0 , 83.5]
Accuracy (%)	57.1 [46.2 , 65.0]	59.5 [48.4 , 68.0]	69.0 [58.0 , 77.4	65.5 [54.3 , 74.8]
PPV (%)	81.8 [64.5 , 93.0]	81.1 [64.8 , 92.0]	84.4 [70.5 , 93.5]	80.4 [66.1 , 90.6]
NPV (%)	41.2 [27.6 , 55.8]	42.6 [28.3 , 57.8]	51.3 [34.8 , 67.6]	47.3 [31.0 , 64.2]
Positive Likelihood Ratio	2.13 [1.00 , 4.54]	2.03 [1.02 , 4.02]	2.57 [1.32 , 4.99]	1.95 [1.11 , 3.43]
Negative Likelihood Ratio	0.68 [0.49 , 0.93]	0.64 [0.45 , 0.91]	0.45 [0.29 , 0.69]	0.53 [0.34 , 0.82]

Table 4. Pair-wise comparison of sensitivity and specificity among each imaging interpretation modalities

4-1. All patients group

Sensitivity (P value) Specificity (p value)	**Multiparametric MRI**	**Integrated ^{18}F-FDG PET/MRI**	**Integrated ^{18}F-choline PET/MRI**	**Multiparametric MRI with ^{18}F-FDG PET/CT**
Multiparametric MRI	-	0.819 0.248	**0.008 0.414	*0.041 0.050
Integrated ^{18}F-FDG PET/MRI	0.819 0.248	-	**0.003 0.527	0.150 0.345
Integrated ^{18}F-choline PET/MRI	**0.008 0.414	**0.003 0.527	-	0.465 0.109
Multiparametric MRI with ^{18}F-FDG PET/CT	*0.041 0.050	0.150 0.345	0.465 0.109	-

Note: Each value is p value from pair-wise comparison of sensitivity or specificity. *, p value under 0.05. ** p value still under 0.05 with Bonferroni correction. Values in the table are the value before Bonferroni correction.

4-2. High Gleason score group

Sensitivity (P value) Specificity (p value)	**Multiparametric MRI**	**Integrated ^{18}F-FDG PET/MRI**	**Integrated ^{18}F-choline PET/MRI**	**Multiparametric MRI with ^{18}F-FDG PET/CT**
Multiparametric MRI	-	0.248 0.180	*0.011 0.157	*0.015 0.025
Integrated ^{18}F-FDG PET/MRI	0.248 0.180	-	*0.016 0.654	0.100 0.479
Integrated ^{18}F-choline PET/MRI	*0.011 0.157	*0.016 0.654	-	0.248 0.256
Multiparametric MRI with ^{18}F-FDG PET/CT	*0.015 0.025	0.100 0.479	0.248 0.256	-

Note: Each value is p value from pair-wise comparison of sensitivity or specificity. *, p value under 0.05. ** p value still under 0.05 with Bonferroni correction. Values in the table are the value before Bonferroni correction.

4-3. Low Gleason score group

Sensitivity (P value) Specificity (p value)	**Multiparametric MRI**	**Integrated ^{18}F-FDG PET/MRI**	**Integrated ^{18}F-choline PET/MRI**	**Multiparametric MRI with ^{18}F-FDG PET/CT**
Multiparametric MRI	-	0.256 0.705	**0.007 0.563	*0.012 0.365
Integrated ^{18}F-FDG PET/MRI	0.256 0.705	-	*0.011 1.00	0.089 0.527
Integrated ^{18}F-choline PET/MRI	**0.007 0.563	*0.011 1.00	-	0.796 0.479
Multiparametric MRI with ^{18}F-FDG PET/CT	*0.012 0.365	0.089 0.527	0.796 0.479	-

Note: Each value is p value from pair-wise comparison of sensitivity or specificity. *, p value under 0.05. ** p value still under 0.05 with Bonferroni correction. Values in the table are the value before Bonferroni correction.

Diagnostic Performance of each Modality

We used three parameters to evaluate the diagnostic performance (accuracy, NND, and DOR).

As aforementioned, integrated ^{18}F-choline PET/MRI provided the best accuracy among all the imaging modalities and in every patient group. Although the difference was not so prominent, integrated ^{18}F-choline PET/MRI showed approximately 12% accuracy increase compared with multiparametric MRI alone in the low Gleason score group (69.0% and 57.1%, respectively). Integrated ^{18}F-FDG PET/MRI and combined interpretation of multiparametric MRI and FDG PET/CT both showed slight improvements in accuracy compared with multiparametric MRI alone, mainly by contributing to the detection of low Gleason score tumors.

Regarding NND, integrated ^{18}F-choline PET/MRI showed the best result (lowest value) in all three patient groups. In addition, the differences of values were accentuated in the low Gleason score group compared with the other groups. Integrated ^{18}F-FDG PET/MRI and combined interpretation of multiparametric MR and FDG PET/CT showed similar NND compared with multiparametric MRI alone. Similar tendencies were observed regarding DOR; however, the DOR of multiparametric MRI in the high Gleason score group was much better than that in the other groups, probably due to the high specificity of multiparametric MRI in the high Gleason score group (Table 5).

Accuracy for Seminal Vesicle Invasion

Among 62 seminal vesicle lobes from the 31 study subjects, 12 sites of seminal vesicle invasion (7 from left lobes, 5 from right lobes) were confirmed by pathologic report. The accuracy for each image interpretation modality is summarized in Table 6. The accuracy of multiparametric MRI was higher than that of any other modality, without significant difference.

.

Detection Rate of Extracapsular Invasion

Among 186 sextants, extracapsular invasion was confirmed in 32 sextants according to the pathologic report. The accuracy rates (the number of sextants in which extracapsular invasion was exactly detected by each image interpretation modality per the total 32 sextants) are presented in Table 7. All the imaging interpretation modalities showed similar accuracy rates.

Table 5. Diagnostic performance presented as number needed to diagnose (NND) and diagnostic odds ratio (DOR) of each modality in each patient group

NND DOR	Multiparametric MRI	Integrated ^{18}F-FDG PET/MRI	Integrated ^{18}F-choline PET/MRI	Multiparametric MRI with ^{18}F-FDG PET/CT
All Patients	2.207 [1.818 , 3.326]	2.306 [1.799 , 3.676]	1.840 [1.518 , 2.590]	2.414 [1.811 , 4.024]
Group	9.475 [3.759 , 24.908]	6.917 [3.094 , 15.762]	11.875 [5.107 , 28.262]	5.854 [2.762 , 11.546]
High Gleason	1.596 [1.486 , 2.355]	1.745 [1.422 , 2.887]	1.508 [1.297 , 2.247]	1.992 [1.504 , 3.746]
Score Group	52.920 [6.928 , 1107]	15.143 [4.255 , 59.119]	27.941 [6.794 , 133.53]	9.254 [2.992 , 25.579]
Low Gleason	3.977 [2.312 , 1782]	3.745 [2.164 , 78.605]	2.455 [1.667 , 6.506]	3.167 [1.888 , 16.602]
Score Group	3.150 [1.002 , 10.295]	3.175 [1.053 , 9.859]	5.714 [1.859 , 18.183]	3.700 [1.274 , 10.970]

Table 6. Detection rates of seminal vesicle invasion in 12 patients

	No. of Detected lesions	**Detection rate (%)**	**False (+)**
Multiparametric MRI	10	83.3	.
Integrated ^{18}F-FDG PET/MRI	9	75.0	1
Integrated ^{18}F-choline PET/MRI	9	75.0	1
Multiparametric MRI with ^{18}F-FDG PET/CT	9	75.0	.

Table 7. Detection rate of extracapsular invasion in 32 sextants which showed pathologic extracapsular invasion

	No. of Answer	**No. of Detected Lesion**	**No. of Missed Lesion**	**Answer Rate (%)**
Multiparametric MRI	17	12	3	53.1
Integrated ^{18}F-FDG PET/MRI	16	12	4	50
Integrated ^{18}F-choline PET/MRI	15	13	4	46.9
Multiparametric MRI with ^{18}F-FDG PET/CT	16	13	3	50

Abbreviations : No. of answer : detect extracapsular invasion correctly; No. of Detected lesion : detect the lesion, but miss extracapsular invasion;
No of Missed lesion : could not detect the lesion.

Discussion

For detection and localization of primary prostate cancer lesions, multiparametric MRI is recommended as the first-line imaging modality. The ESUR guideline suggests that the detection and staging protocol of multiparametric MRI should include T2WI, DWI, and DCE, and optional MR spectroscopy (*24*). However, previous studies showed conflicting results regarding the detection or localization ability of multiparametric MRI. Haider et al. (*25*) reported that adding DWI to T2WI improved sensitivity of localization compared with T2WI alone, whereas specificity was slightly decreased. While some studies suggested that adding DWI to T2WI improved prostate cancer localization performance (*26*, *27*), another study indicated that DWI did not add value for localization of prostate cancer (*28*). Delongchamps et al. (*3*) suggested that multiparametric MRI increased the detection performance of prostate cancer in the peripheral zone, but failed to do the same in the transitional zone.

PET/MRI is another option for cancer detection and localization, and provides metabolic information (high inherent sensitivity of PET) without adversely affecting the merits of multiparametric MRI such as fine anatomical allocation and functional information. The first commercially available PET/MRI equipment consisted of tandem system scanners, and fully

integrated PET/MRI scanners followed (*29*). Overcoming potential technical considerations such as MR-based attenuation correction (AC), motion correction, and MR-compatible PET detectors has improved the technical feasibility of PET/MRI for prostate cancer (*13-17*, *30*, *31*). In particular, integrated PET/MRI scanners with MR-compatible PET detectors (avalanche photodiode detectors) are nearly free of misregistration and allow simultaneous acquisition of PET and MRI data (*29*). The present study was based on previous investigations and evaluated for the first time the detection/localization performance of PET/MRI in a fully integrated PET/MRI system compared with multiparametric MRI and combined interpretation of multiparametric MRI and ^{18}F-FDG PET/CT in an actual clinical setting. This was also the first study that compared detection/localization performance of different radiotracers (^{18}F-fluorocholine and ^{18}F-FDG) on the basis of detection and sector-based localization of prostate cancer.

Compared with multiparametric MRI alone, integrated ^{18}F-choline PET/MRI showed statistically superior sensitivity without significant decrease of specificity, regardless of Gleason score. Integrated ^{18}F-FDG PET/MRI also showed enhanced sensitivity without significant decrease of specificity, although there was no statistical significance. Furthermore, regarding diagnostic performance represented as accuracy, NND, and DOR, integrated ^{18}F-choline PET/MRI improved the diagnostic performance compared with

multiparametric MRI alone. Integrated ^{18}F-FDG PET/MRI showed slightly better accuracy compared with multiparametric MRI alone, but failed to yield an improvement of NND and DOR. Previous study results that revealed that ^{18}F-choline uptake showed high sensitivity for prostate cancer detection (*32*) but decreased specificity due to nonspecific uptake in benign prostate lesions (*33*) were similar to our results. Additionally, our results showed that the increase in sensitivity was more prominent (statistically significant) than the decrease in specificity (statistically insignificant), and led to improved accuracy, NND, and DOR. Previous studies about localization of prostate cancer using 3 T multiparametric MRI showed a 68–88% sensitivity, 67–100% specificity, and 70–94% accuracy (*30*, *34*). Previous studies using ^{18}F-choline PET/MRI in tandem system PET/MRI scanners showed 79%, 70%, and 75% for sensitivity, specificity, and accuracy (*30*), and 66%, 82%, and 72% for sensitivity, specificity, and accuracy in separate acquisition with post hoc image fusion (*31*), respectively. Our statistics showed similar results to the previous studies, including the results of multiparametric MRI and integrated PET/MRI images. Although there was much overlap in accuracy between multiparametric MRI and ^{18}F-choline PET/MRI in previous studies, the use of integrated ^{18}F-choline PET/MRI in our study resulted in improved accuracy in the detection/localization of prostate cancer.

Generally, in the high Gleason score group, all the imaging interpretation modalities showed similar accuracy and NND. Multiparametric MRI showed

a high specificity of up to 96.4% and similar sensitivity compared with radiotracer-using images, and consequently showed better PPV, meaningful positive likelihood ratio (18.54), and better DOR (52.920). We suggest that the low +LR with PET was caused by hyperplastic nodules or nonspecific inflammatory lesions, which can show uptake on PET and low signal intensity on T2 weighted images, with resultant confusion. This overlap was probably more prominent in the case of ^{18}F-FDG PET/MRI.

Interestingly, integrated ^{18}F-choline PET/MRI showed marginally positive results in some aspects in the low Gleason score group. Compared with multiparametric MR, only integrated ^{18}F-choline PET/MRI could provide significantly high sensitivity (66.7% versus 47.4%, $p = 0.007 \times 10^{6}$) after Bonferroni correction. It also presented better accuracy (69.0% versus 57.1%), NND (2.455 versus 3.977), and DOR (5.714 versus 3.150). Although the differences were slight, diagnostic performance (accuracy, NND, and DOR) was credibly better with integrated ^{18}F-choline PET/MRI than multiparametric MRI. Our result might have been affected by the different mechanisms of lesion visualization between choline PET and multiparametric MRI (especially ADC). The biologic basis for radiolabeled choline uptake in tumors is the malignancy-induced upregulation of choline kinase, which leads to the incorporation and trapping of choline in the form of phosphatidylcholine (lecithin) in the tumor cell membrane (*7*). Meanwhile, the ADC value as a functional marker is based on the assessment of Brownian

motion of extracellular water molecules (*30*). Studies using ^{18}F-choline PET/MRI conducted by de Parrot et al. (*30*) and Wetter et al. (*35*) showed no significant correlation between ADC and choline SUV, meaning that the choline SUV and ADC values derived from ^{18}F-choline PET/MRI in prostate cancer reflect different parts of tumor pathophysiology. In addition, there was no significant correlation between Gleason score and choline SUV (*29*, *36*). However, Park et al. (*14*) suggested that there was a correlation between choline SUV combined with ADC value and Gleason score. Considering the results mentioned above, we suggest that ^{18}F-choline PET/MRI can contribute additional or compensatory value in the evaluation of well-differentiated or low Gleason tumors because of the synergy between choline PET and multiparametric MRI (especially ADC). This point requires further evaluation in the domains of basic biology and large-population clinical medicine. In Korea, most prostate MRI studies are performed after TRUS-guided biopsy because of National Health Insurance protocols. Consequently, integrated ^{18}F-choline PET/MRI can be selectively applied, which improves detection/localization, if the biopsy result is a low Gleason score prostate cancer.

An important theme of our study was evaluating the diagnostic performance of integrated PET/MRI in an actual clinical setting; therefore, integrated PET/MRI was compared with combined interpretation of multiparametric MRI and PET/CT, which is widely used for preoperative

detection, localization, and staging of prostate cancer. Generally, sensitivity, specificity, accuracy, NND, and DOR were similar with integrated ^{18}F-FDG PET/MRI and combined interpretation of multiparametric MRI and ^{18}F-FDG PET/CT, regardless of Gleason score. We adopted only the 3D-Dixon VIBE sequence-based soft-tissue AC without ultrashort echo time sequences, and the pelvic bone was not considered in our MR-based AC (*29*). This could have led to underestimation of the attenuation effect of bone—SUVs of soft-tissue lesions close to bone could have been underestimated by up to 4% (*37*, *38*). However, according to our results, AC in integrated PET/MRI is compatible with conventional CT-based AC. This would explain the similar results for integrated ^{18}F-FDG PET/MRI and combined interpretation of MRI and PET/CT. On the other hand, although statistical significance was not achieved, integrated ^{18}F-choline PET/MRI presented higher sensitivity and specificity than did combined interpretation of MRI and PET/CT in all three patient groups, resulting in greater improvement in diagnostic performance (NND and DOR), regardless of Gleason score. As the soft-tissue contrast of CT is inferior to that of MRI, and as MR-based fusion images could provide more precise anatomical allocation than separate MRI and PET/CT images, we anticipated that integrated PET/MRI would perform better in the detection and localization of primary cancer lesions in the prostate. This hypothesis was consequently supported by the aforementioned result. Moreover, we suggested that more prominent uptake of ^{18}F-choline in human prostate cancer

lesions compared with ^{18}F-FDG (*39*) could partly contribute to the aforementioned result, as discussed below. Furthermore, if the feasibility and capacity of whole-body integrated PET/MRI for evaluation of lymph node and focal metastatic lesions could be proven, both ^{18}F-choline and ^{18}F-FDG integrated PET/MRI could replace MRI and PET/CT in preoperative evaluation of prostate cancer with the inherent advantages of one-stop imaging and non-exposure to radiation from CT scanners. Thus, we anticipate that these modalities will be beneficial for preoperative patients or active surveillance patients who need frequent follow-up imaging.

Comparing the two radiotracer-based imaging modalities, integrated ^{18}F-choline PET/MRI presented higher sensitivity, accuracy, NND, and DOR than did ^{18}F-FDG imaging in all patient groups. Research conducted by Price et al. showed that the ^{18}F-choline uptake in prostate cancer lesions showed higher SUV than the ^{18}F-FDG uptake in humans, regardless of the tumor's androgen sensitivity (*39*). In contrast, glucose transporter 1 (GLUT1) gene expression level was higher in a poorly differentiated androgen-independent cell line than in a well-differentiated hormone-sensitive cell line, suggesting that the level of glucose uptake increases with progression of malignancy grade (*7*). Furthermore, under aerobic conditions, both androgen-sensitive and androgen-independent prostate tumors showed higher choline than ^{18}F-FDG uptake. However, during hypoxia, the tumor uptake of ^{18}F-FDG is higher than that of choline (*40*). Because organ-confined prostate cancer is usually less

malignant, castration-sensitive, and less necrotic (less hypoxic), it can be inferred from the above studies that choline PET/MRI can be more helpful than FDG PET/MRI in prostate cancer, particularly low Gleason score tumors, as shown by our results. In addition, as aforementioned, glucose consumption of prostate cancer is relatively low compared with other cancers (*7*), and this may partly explain this result. Thus, if the systemic biopsy results reveal a low Gleason score tumor, choline PET/MRI can be considered a better imaging modality than FDG PET/MRI for further evaluation.

The researchers expected that integrated PET/MRI would be useful for the detection of seminal vesicle invasion or extracapsular invasion of prostate cancer, because of the high intrinsic sensitivity of PET. However, both ^{18}F-choline and ^{18}F-FDG integrated PET/MRI showed similar accuracy rates regarding seminal vesicle and extracapsular invasion compared with multiparametric MRI or combined interpretation of MRI and ^{18}F-FDG PET/CT. General accuracy of PET/MRI for detection of extracapsular extension was 46.9–50%, which was slightly lower than but similar to that of previous study (63.1%) (*31*). This result implies that MR imaging could potentially play a more critical role in the determination of seminal vesicle or extracapsular invasion, but that radiologists do not regard all the hyperuptake area as real tumor extent, particularly in the peripheral boundary of hypermetabolic uptake lesions (Tables 6 and 7).

There are also some limitations in our study. First, the study population included only patients who were diagnosed with prostate cancer on TRUS-guided biopsy and planned to undergo surgery. Thus, the enrolled patient group did not represent the universal population. Furthermore, the sensitivity and negative predictive values could have been overestimated because the reviewers were aware that the study population consisted of cancer patients. However, comparing our results to those of previous studies, the sensitivity value was not markedly deviated (*11*, *17*, *30*, *31*, *34*). Second, although we suggested using choline PET/MRI for the detection and localization of primary prostate cancer lesions, the number of subjects in the study population was relatively small due to the limited study period. Further prospective investigation with larger study populations will be needed for validation. Finally, although we used whole-mount mapping of the prostate specimens, the slices of the specimen did not exactly match the MRI axial images because of differences in axis and slice/section thickness between the pathologic slide and PET/MRI. Consequently, the abnormal focal lesions on PET/MRI might not have matched the true tumor focus on the pathologic map/slices. The researchers matched MRI axial images and pathologic slices with consensus to address this problem.

In summary, integrated PET/MRI performed with a dedicated integrated PET/MRI scanner is expected to provide reasonable accuracy and diagnostic performance in the detection/localization of prostate cancer. Regarding the

low Gleason score cancers, integrated PET/MRI using ^{18}F-choline as the radiotracer has significantly higher sensitivity than multiparametric MRI alone, and has the potential to provide better accuracy and diagnostic performance compared with other imaging interpretation modalities. Generally, integrated ^{18}F-choline PET/MRI shows better accuracy and diagnostic performance than integrated ^{18}F-FDG PET/MRI, regardless of Gleason score. If the value of integrated PET/MRI for loco-regional or distant nodal/organ metastasis is confirmed, integrated PET/MRI imaging may be a good alternative (in the case of integrated ^{18}F-FDG PET/MRI) or potentially better imaging tool, particularly in low Gleason score patients (in the case of integrated ^{18}F-choline PET/MRI), than MRI and PET/CT for preoperative evaluation of prostate cancer, with the inherent advantages of one-stop imaging and non-exposure to radiation from CT scanners.

References

1. World Cancer Research Fund International. Cancer statistics worldwide. 2014 [cited 2014 April 12]; Available from: http://www.wcrf.org/cancer_statistics/world_cancer_statistics.php.

2. Korea National Cancer Information Center. Cancer statistics. 2014 [cited 2014 April 12]; Available from: http://www.cancer.go.kr/mbs/cancer/subview.jsp?id=cancer_040102000000.

3. Delongchamps NB, Rouanne M, Flam T, et al. Multiparametric magnetic resonance imaging for the detection and localization of prostate cancer: combination of T2-weighted, dynamic contrast-enhanced and diffusion-weighted imaging. BJU international. 2011;107(9):1411-8.

4. Bonekamp D, Jacobs MA, El-Khouli R, Stoianovici D, Macura KJ. Advancements in MR imaging of the prostate: from diagnosis to interventions. Radiographics : a review publication of the Radiological Society of North America, Inc. 2011;31(3):677-703.

5. Watanabe H, Kanematsu M, Kondo H, et al. Preoperative detection of prostate cancer: a comparison with 11C-choline PET, 18F-fluorodeoxyglucose PET and MR imaging. Journal of magnetic resonance imaging : JMRI. 2010;31(5):1151-6.

6. Kozlowski P, Chang SD, Jones EC, Berean KW, Chen H,

Goldenberg SL. Combined diffusion-weighted and dynamic contrast-enhanced MRI for prostate cancer diagnosis--correlation with biopsy and histopathology. Journal of magnetic resonance imaging : JMRI. 2006;24(1):108-13.

7. Jadvar H. Prostate cancer: PET with 18F-FDG, 18F- or 11C-acetate, and 18F- or 11C-choline. Journal of nuclear medicine. 2011;52(1):81-9.

8. Takahashi N, Inoue T, Lee J, Yamaguchi T, Shizukuishi K. The roles of PET and PET/CT in the diagnosis and management of prostate cancer. Oncology. 2007;72(3-4):226-33.

9. Scher B, Seitz M, Albinger W, et al. Value of 11C-choline PET and PET/CT in patients with suspected prostate cancer. European journal of nuclear medicine and molecular imaging. 2007;34(1):45-53.

10. Farsad M, Schiavina R, Castellucci P, et al. Detection and localization of prostate cancer: correlation of ^{11}C-choline PET/CT with histopathologic step-section analysis. Journal of nuclear medicine 2005;46(10):1642-9.

11. Testa C, Schiavina R, Lodi R, et al. Prostate cancer: sextant localization with MR imaging, MR spectroscopy, and 11C-choline PET/CT. Radiology. 2007;244(3):797-806.

12. Martorana G, Schiavina R, Corti B, et al. 11C-choline positron emission tomography/computerized tomography for tumor localization of primary prostate cancer in comparison with 12-core biopsy. The Journal of

urology. 2006;176(3):954-60; discussion 60.

13. Souvatzoglou M, Eiber M, Martinez-Moeller A, et al. PET/MR in prostate cancer: technical aspects and potential diagnostic value. European journal of nuclear medicine and molecular imaging. 2013;40(1):79-88.

14. Park H, Wood D, Hussain H, et al. Introducing parametric fusion PET/MRI of primary prostate cancer. Journal of Nuclear Medicine. 2012;53(4):546-51.

15. Jambor I, Borra R, Kemppainen J, et al. Improved detection of localized prostate cancer using co-registered MRI and 11C-acetate PET/CT. European journal of radiology. 2012;81(11):2966-72.

16. Souvatzoglou M, Eiber M, Takei T, et al. Comparison of integrated whole-body [11C]choline PET/MR with PET/CT in patients with prostate cancer. European journal of nuclear medicine and molecular imaging. 2013;40(10):1486-99.

17. Wetter A, Lipponer C, Nensa F, et al. Simultaneous 18F choline positron emission tomography/magnetic resonance imaging of the prostate: initial results. Investigative radiology. 2013;48(5):256-62.

18. Kang DE, Fitzsimons NJ, Presti JC, Jr., et al. Risk stratification of men with Gleason score 7 to 10 tumors by primary and secondary Gleason score: results from the SEARCH database. Urology. 2007;70(2):277-82.

19. Makarov DV, Sanderson H, Partin AW, Epstein JI. Gleason score 7 prostate cancer on needle biopsy: is the prognostic difference in Gleason

scores 4 + 3 and 3 + 4 independent of the number of involved cores? The Journal of urology. 2002;167(6):2440-2.

20. Stark JR, Perner S, Stampfer MJ, et al. Gleason score and lethal prostate cancer: does 3 + 4 = 4 + 3? Journal of clinical oncology : official journal of the American Society of Clinical Oncology. 2009;27(21):3459-64.

21. Hawass NE. Comparing the sensitivities and specificities of two diagnostic procedures performed on the same group of patients. The British journal of radiology. 1997;70(832):360-6.

22. Glas AS, Lijmer JG, Prins MH, Bonsel GJ, Bossuyt PM. The diagnostic odds ratio: a single indicator of test performance. Journal of clinical epidemiology. 2003;56(11):1129-35.

23. How Good is That Test? (II). Bandolier Journal. May 1996 ed. Oxford: Oxford University Press, 1996; p. 1-2.

24. Barentsz JO, Richenberg J, Clements R, et al. ESUR prostate MR guidelines 2012. European radiology. 2012;22(4):746-57.

25. Haider MA, van der Kwast TH, Tanguay J, et al. Combined T2-weighted and diffusion-weighted MRI for localization of prostate cancer. AJR American journal of roentgenology. 2007;189(2):323-8.

26. Kim CK, Park BK, Lee HM, Kwon GY. Value of diffusion-weighted imaging for the prediction of prostate cancer location at 3T using a phased-array coil: preliminary results. Invest Radiol. 2007;42(12):842-7.

27. Lim HK, Kim JK, Kim KA, Cho KS. Prostate cancer: apparent

diffusion coefficient map with T2-weighted images for detection--a multireader study. Radiology. 2009;250(1):145-51.

28. Vargas HA, Akin O, Franiel T, et al. Diffusion-weighted endorectal MR imaging at 3 T for prostate cancer: tumor detection and assessment of aggressiveness. Radiology. 2011;259(3):775-84.

29. Quick HH. Integrated PET/MR. JMRI. 2014;39(2):243-58.

30. de Perrot T, Rager O, Scheffler M, et al. Potential of hybrid ^{18}F - fluorocholine PET/MRI for prostate cancer imaging. European journal of nuclear medicine and molecular imaging. 2014;41(9):1744-55.

31. Hartenbach M, Hartenbach S, Bechtloff W, et al. Combined PET/MRI improves diagnostic accuracy in patients with prostate cancer: a prospective diagnostic trial. Clinical cancer research : an official journal of the American Association for Cancer Research. 2014;20(12):3244-53.

32. Umbehr MH, Muntener M, Hany T, Sulser T, Bachmann LM. The role of 11C-choline and 18F-fluorocholine positron emission tomography (PET) and PET/CT in prostate cancer: a systematic review and meta-analysis. European urology. 2013;64(1):106-17.

33. Li X, Liu Q, Wang M, et al. C-11 choline PET/CT imaging for differentiating malignant from benign prostate lesions. Clinical nuclear medicine. 2008;33(10):671-6.

34. C. M. A. Hoeks et al. Prostate Cancer: Multiparametric MR Imaging for Detection, Localization, and Staging. Radiology 2011; 261(1); 46-66

35. Wetter A, Nensa F, Schenck M, et al. Combined PET imaging and diffusion-weighted imaging of intermediate and high-risk primary prostate carcinomas with simultaneous ^{18}F-choline PET/MRI. PloS one. 2014;9(7):e101571

36. Breeuwsma AJ, Pruim J, Jongen MM, et al. In vivo uptake of [11C]choline does not correlate with cell proliferation in human prostate cancer. European journal of nuclear medicine and molecular imaging. 2005;32(6):668-73.

37. Samarin A, Burger C, Wollenweber SD, et al. PET/MR imaging of bone lesions--implications for PET quantification from imperfect attenuation correction. European journal of nuclear medicine and molecular imaging. 2012;39(7):1154-60.

38. Akbarzadeh A, Ay MR, Ahmadian A, Alam NR, Zaidi H. MRI-guided attenuation correction in whole-body PET/MR: assessment of the effect of bone attenuation. Annals of nuclear medicine. 2013;27(2):152-62.

39. Price DT, Coleman RE, Liao RP, Robertson CN, Polascik TJ, DeGrado TR. Comparison of ^{18}F-fluorocholine and ^{18}F-fluorodeoxyglucose for positron emission tomography of androgen dependent and androgen independent prostate cancer. The Journal of urology. 2002;168(1):273-80.

40. Hara T, Bansal A, DeGrado TR. Effect of hypoxia on the uptake of [methyl-3H]choline, [1-^{14}C] acetate and [^{18}F]FDG in cultured prostate cancer cells. Nuclear medicine and biology. 2006;33(8):977-84.

국문 초록

연구목적 : 일체형 PET/MRI 기기를 이용하여 촬영한 PET/MRI 융합영상을 기존 다변수 자기공명영상(multiparametric MRI) 및 PET/CT 영상과 비교하여 전립선암 병변의 검출 및 국소화에 대한 진단능을 알아보고자 한다.

방법 : 이 후향적 연구는 임상연구윤리위원회의 승인을 받았다. 새로이 전립선암으로 진단되고 전립선 전절제술을 받은 총 31명의 환자군이 연구에 포함되었다. 상기 환자군에 대하여 수술 전 ^{18}F-choline PET/MRI 융합영상과 ^{18}F-FDG PET/MRI 융합영상을 각각 일체형 PET/MRI 기기를 이용하여 촬영하였고, ^{18}F-FDG PET/CT 를 촬영하였다. 영상소견 분석 시 전립선을 6개의 구역으로 나누어 분석하였으며, 3명의 비뇨생식기계 영상의학과 전문의가 각 구역의 종양의 존재 여부를 4개의 서로 다른 영상기법별로 평가하였다. (1. 다변수 자기공명영상; 2. ^{18}F-FDG PET/MRI 융합영상과 다변수 자기공명영상의 동시판독; 3. ^{18}F-Choline PET/MRI 융합영상과 다변수 자기공명영상의 동시판독. 4. 다변수 자기공명영상

과 ^{18}F−FDG PET/CT 의 동시판독). 민감도, 특이도, 정확도, 양성 및 음성예측도와 양성 및 음성우도비를 각 영상기법별로 평가하였으며, DOR (diagnostic odds ratio) 및 NND (number needed to diagnose) 을 구하여 진단능을 평가하였다. 정낭의 침범 여부 및 각 구역별 피막 외 침범 역시 평가하였다. 상기 평가 척도들은 수술 후 병리소견을 기준으로 하였다.

결과 : ^{18}F−choline PET/MRI 융합영상은 전체 환자군 및 낮은 글리슨 점수 환자군에서 다변수 자기공명영상에 비하여 통계적으로 높은 민감도를 보였다. 다변수 자기공명영상과 PET/CT 의 동시판독과 비교하여, ^{18}F−choline PET/MRI 및 ^{18}F−FDG PET/MRI 은 민감도 및 특이도에 있어 차이를 보이지 않았다. 그러나 ^{18}F−choline PET/MRI 융합영상은 다른 영상기법과 비교하여 글리슨 점수에 상관없이 가장 좋은 진단능 (정확도, NND 및 DOR) 을 보였다. 또한 ^{18}F−choline PET/MRI 융합영상은 ^{18}F−FDG PET/MRI 융합영상에 비해 더 좋은 민감도와 진단능을 보인다

결론 : 다변수 자기공명영상과 ^{18}F−choline PET/MRI 융합영상의 동시 판독은 전립선암 병변의 검출 및 국소화에 있어 기존의 방법과 비교하여 동등한 민감도, 특이도 및 더 좋은 진단능을 제공한다.

키워드 : 자기공명영상, 양전자방출단층촬영, 융합영상, 전립선암, 진단능

학번 : 2010-21812